nature communications

Article

https://doi.org/10.1038/s41467-025-58363-8

Molecular basis for the regulation of human phosphorylase kinase by phosphorylation and Ca^{2+}

Received: 11 August 2024

Accepted: 20 March 2025

Ruifang Ma[1,7], **Bowen Du**[1,7], **Chen Shi**[2,3,7], **Lei Wang**[1], **Fuxing Zeng**[4,5], **Jie Han**[1], **Huiyi Guan**[1], **Yong Wang**[2,6] ✉ & **Kaige Yan**[1,5] ✉

Phosphorylase kinase (PhK) regulates the degradation of glycogen by integrating diverse signals, providing energy to the organism. Dysfunctional mutations may directly lead to Glycogen Storage Disease type IX (GSD IX), whereas the abnormal expression of PhK is also associated with tumors. Here, we use cryo-electron microscopy (cryo-EM) to resolve its near-atomic structures in the inactive and active states. These structures reveal the interactions and relative locations of the four subunits (αβγδ) within the PhK complex. Phosphorylated α and β subunits induce PhK to present a more compact state, while Ca^{2+} causes sliding of the δ subunit along the helix of the γ subunit. Both actions synergistically activate PhK by enabling the de-inhibition of the γ subunit. We also identified different binding modes between PhK and its substrate, glycogen phosphorylase (GP), in two distinct states, using cross-linking mass spectrometry (XL-MS). This study provides valuable insights into the regulatory mechanisms of PhK, thereby enhancing our understanding of GSD IX and its implications in tumorigenesis.

Glycogen is the main storage form of glucose in animals and humans, which plays a crucial role in regulating blood sugar levels and ensuring a steady supply of energy to the body[1]. The breakdown of glycogen in tissues is controlled through the action of several protein kinases and phosphatases. PhK plays a key role in the cascade system for regulating glycogen metabolism. It phosphorylates a single serine residue of glycogen phosphorylase (GP), catalyzing the conversion of inactive phosphorylase b (GPb) into active phosphorylase a (GPa)[2]. GPa catalyzes the degradation of glycogen, ultimately generating energy to support a broad range of cellular activities in most tissues[3].

PhK is an $(\alpha\beta\gamma\delta)_4$ hexadecameric enzyme complex of 1.3 MDa, where α, β, and δ are regulatory subunits, and γ is the catalytic subunit. The γ (~45 kDa) subunit can be divided into an N-terminal kinase domain and a C-terminal regulatory domain that contains high-affinity calmodulin (CaM) binding sites[4,5]. When responding to various physiological signals and hormonal stimuli, the α (~138 kDa) and β (~125 kDa) subunits are phosphorylated by cyclic AMP-dependent protein kinase (PKA), thereby leads to the activation of PhK[6,7]. The δ (16.7 kDa) subunit is an endogenous molecule of CaM and it mediates the regulation of PhK activity by Ca^{2+} derived from neuronal stimulation[8,9]. All of these factors position PhK as a central point for the regulation of glycogen metabolism. Individually, either Ca^{2+} binding to δ subunit or phosphorylation of the α- and β-subunits partially activates PhK, but their synergistic action can effectively activate PhK[10]. In vitro, pH is an additional factor that modulates activity. PhK exhibits low activity at pH 6.8, but experiences a notable increase in activity at

---

[1]Shenzhen Key Laboratory of Biomolecular Assembling and Regulation, School of Life Sciences, Southern University of Science and Technology, Shenzhen 518055, China. [2]College of Life Sciences, Zhejiang University, Hangzhou 310058, China. [3]Department of Engineering Mechanics, Zhejiang University, Hangzhou 310027, China. [4]Department of Systems Biology, School of Life Sciences, Southern University of Science and Technology, Shenzhen 518055, China. [5]Institute for Biological Electron Microscopy, Southern University of Science and Technology, Shenzhen 518055, China. [6]The Provincial International Science and Technology Cooperation Base on Engineering Biology, International Campus of Zhejiang University, Haining 314499, China. [7]These authors contributed equally: Ruifang Ma, Bowen Du, Chen Shi. ✉e-mail: yongwang_isb@zju.edu.cn; yankg@sustech.edu.cn

pH 8.2, while Ca^{2+} dependence is retained. The activity of PhK at pH 6.8 can be significantly enhanced (by 10-20 folds) through phosphorylation or limited proteolysis, whereas its activity remains largely unchanged at pH 8.2[10,11]. Furthermore, some small molecule signals, like ADP, ATP, and Mg^{2+}, also stimulate PhK activity[11–13].

The α and γ subunits of PhK exhibit tissue specificity, primarily presenting as skeletal muscle type (α1, γ1) and liver type (α2, γ2)[14]. Inherited PhK deficiency leads to Glycogen Storage Disease type IX (GSD IX), constituting approximately 25% of the total individuals with GSD[15]. GSD IX is primarily characterized by the accumulation of muscle glycogen and hepatic glycogen, causing clinical symptoms such as muscle weakness, exercise intolerance, hepatomegaly, delayed childhood development, and liver dysfunction[16]. Additionally, PhK deficiency, which also leads to cardiac glycogenosis, is relatively rare but typically results in fatality during infancy[17]. In addition, the aberrant expression of PhK is also closely associated with the growth and migration of tumors. Camus et al. through analysis of The Cancer Genome Atlas database, found that the proportion of at least one subunit in the full enzyme of PhK exhibiting mutations in tumors varies from 59% (ovarian serous cystadenocarcinoma) to 97% (lung squamous cell carcinoma)[18]. Aberrant expression of PhK components has been observed to impact the growth and migration of tumors in colorectal cancer patient tissues, mouse, and zebrafish models[18–20]. Therefore, PhK serves as an excellent prognostic marker and drug target for tumors.

Despite being the first protein kinase to be discovered and purified[21], the structure and regulation of PhK remain poorly understood due to its large size and complexity. In this study, we report the cryo-EM structures of human muscle PhK in the inactive state and active state. Together with cross-linking mass spectrometry (XL-MS), our work provides a structural basis for the activation mechanism and substrate recruitment of PhK, which is essential for understanding the disease mechanisms of PhK-related diseases.

Results

We obtained the full-length human muscle PhK (hPhK) through recombinant expression in HEK293F cells (Supplementary Fig. 1). Subsequently, we solved the cryo-EM structures of hPhK under two conditions using high-quality recombinant protein: (1) the dephosphorylation state without Ca^{2+} (denoted as inactive hPhK); (2) the phosphorylation state in the presence of Ca^{2+} (denoted as active hPhK), at 4.2 and 3.7 Å overall resolution, respectively (Supplementary Figs. 2–3 and Supplementary Table 1). To explore the specific details of each subunit in the inactive state, we obtained an additional high-resolution structure with a resolution of 3.4 Å (Supplementary Fig. 4). Furthermore, we conducted local refinement to enhance the local resolution of hPhK.

Structure of human muscle PhK

From the global structure, the front view of hPhK resembles a butterfly (Fig. 1a, b), which is consistent with the previously reported rabbit muscle PhK structure[22], having dimensions of 320 × 220 × 165 Å (Fig. 1a). The side views of hPhK present a chalice-like shape (Fig. 1a, middle) and a cuboid shape (Fig. 1a, right). The β subunit constitutes the body of the butterfly, while the αγδ heterotrimer forms the wings, and the two are connected through the α subunit (Fig. 1c).

Structurally, PhK is actually a dimeric assembly comprised of two $(\alpha\beta\gamma\delta)_2$ octamers[23].The connection between these octamers is achieved through 'bridges' that are formed by four β subunits (β_4) spanning across (Fig. 1d). Based on our cryo-EM structure, we classify the α and β subunits into five domains (named D1-D5) (Supplementary Fig. 5a). The $(\alpha\beta\gamma\delta)_2$ octamer is connected via the α-β-α-β heterotetramer (Supplementary Fig. 5b). The β4 tetramer exhibits D4 symmetry, and each β-subunit connects with two other subunits primarily through the $D1_\beta$ and $D5_\beta$ domains (Fig. 1d). The α-β-α-β heterotetramer is primarily maintained by polar interactions among $D1_\alpha$, $D2_\alpha$, $D1_\beta$, and $D2_\beta$ (Supplementary Fig. 5b).

Autoinhibition structure of γ subunit in the inactive state

In terms of functionality, the γ subunit can be divided into two parts: the catalytic kinase domain (CKD) and the autoregulatory domain (ARD). Like other kinases, the CKD region is composed of a smaller ATP-binding domain (N-lobe) and a larger substrate-binding domain (C-lobe), which are connected to form a typical bilobed catalytic core. Furthermore, the ARD region can be divided into the CaM binding domain (CBD) and the autoinhibitory domain (AID) (Fig. 2a). The γ subunit is anchored to both ends of the α subunit through the AID regions and the N-lobe of CKD region, thereby ensuring a more stable binding in the inactive state (Supplementary Fig. 6). There are also interactions between the C-lobe of the CKD region and the AID region. The hydrogen bonds formed by $Trp231_\gamma/Gln363_\gamma$, $Trp231_\gamma/Asn366_\gamma$, and $His232_\gamma/Gln363_\gamma$ stabilize the interaction between the two regions (Fig. 2b). The γ-AID region typically serves as a pseudosubstrate in other members of the Ca^{2+}/Calmodulin-dependent protein kinases (CaMKs), inhibiting the kinase activity. Previous studies have obtained the crystal structure of γ-CKD region with a modified peptide substrate (MC peptide)[24]. In our inactivated state structure, we observed that the AID region is located in the protein-substrate pocket, and residues $Lys360_\gamma$, $Lys361_\gamma$, and $Gly362_\gamma$ have clashes with the -3 and -2 sites of the MC peptide (Fig. 2c). This suggests that the AID region in hPhK also mimics a peptide target of the enzyme, thus blocking the substrate-binding site and causing the enzyme to be in an autoinhibited state.

Structure of δ subunit without Ca^{2+}

The δ subunit, CaM, binds tightly to γ subunit even in the absence of Ca^{2+}. The pocket of apo/CaM, which binds to γ-CBD, is highly conserved (Fig. 2d). Apo/CaM embraces the helix of γ-CBD in an antiparallel orientation through extensive interactions, with the CaM N-lobe binding the C-terminal portion and the C-lobe binding the N-terminal portion of γ-CBD (Fig. 2e). This compact structure buries a total surface area of ~2800 $Å^2$, similar to the surface area buried by other CaM-helix complexes[25]. Meanwhile, residues $Phe305_\gamma$ and $Ala309_\gamma$ insert into the C-lobe hydrophobic pocket, and Ala314γ and Ile318γ insert into the N-lobe hydrophobic pocket of CaM (Fig. 2e). Additionally, amino acids from the γ-CKD region engage in interactions with CaM (Fig. 2f). Typically, apo/CaM binds to helices in an extended conformation and antiparallel orientation, whereas Ca^{2+}/CaM binds in a compact conformation and parallel orientation[25,26]. However, the endogenous apo/CaM in the PhK complex exhibits a similar compact structure to Ca^{2+}/CaM, but in the antiparallel orientation. This compact structure of Apo/CaM and its high binding affinity with the γ-CKD region provide insights into how endogenous CaM sustains tight binding even in the absence of Ca^{2+}.

Analysis of the phosphorylation sites of hPhK

In rabbits, Ser1018 on the α subunit and serines 26 and 700 on the β subunit can be phosphorylated by PKA. Meanwhile, within the α subunit, three self-phosphorylation sites (serines 972, 985, 1007), which are phosphorylated by PhK itself, along with four endogenous phosphorylation sites (serines 1020, 1023, 1030, 1042) that are naturally phosphorylated by other kinases within the cell, have been identified. Additionally, in the β subunit, only two self-phosphorylation sites (Ser11 and Ser1088) have been identified[12,27]. To gain a deeper understanding of the phosphorylation sites following PKA treatment, we employed tandem mass spectrometry (MS/MS) for precise mapping of the phosphorylation sites within hPhK (Fig. 3a, b). As expected, both PKA phosphorylation sites and self-phosphorylation sites were identified, with the exception of 1088_β, as this position does not align with a serine residue in hPhK (Supplementary Fig. 7a). However, not all

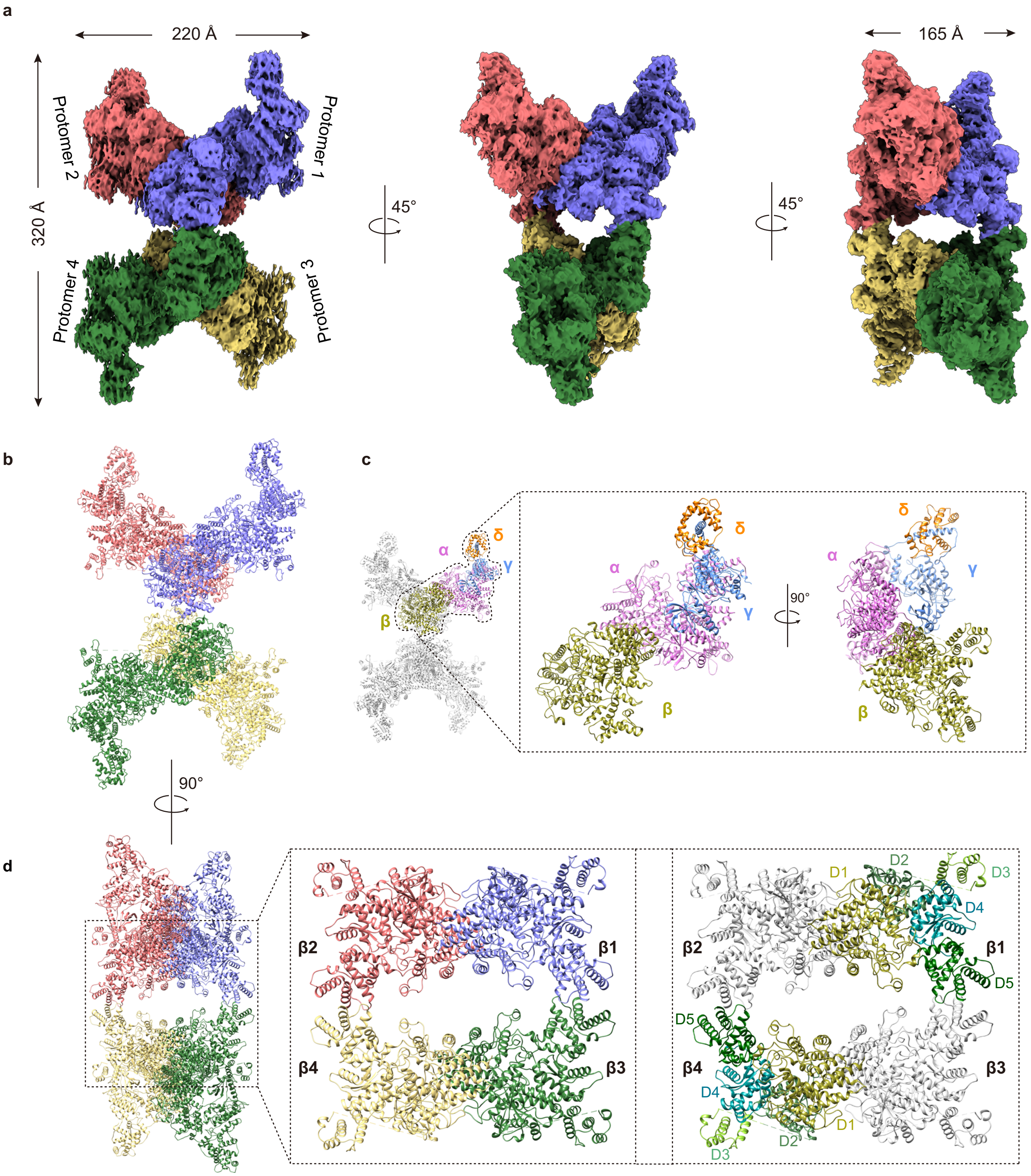

Fig. 1 | Cryo-EM structure of inactive hPhK. a Different views of hPhK. The four hPhK protomers are represented in slateblue, salmon, green, and yellow, respectively. Left, front view (butterfly orientation). Middle, side view (chalice orientation), rotated 45° along the vertical axis from the butterfly orientation. Right, side view (tetrad orientation), rotated 45° along the vertical axis from the chalice orientation. **b** Overall view of the atomic models of hPhK. **c** Location of four subunits (αβγδ) from one protomer and the relative positions of the αβγδ subunits. **d** Structure of the central core formed by the β_4 homotetramer. Left, the overall location of four β subunits, rotated 90° along the vertical axis from (**b**). Middle, an enlarged view of the four β subunits. Right, an enlarged view of the four β subunits, and the five domains of β1 and β4 subunits are shown in different shades of green.

endogenous phosphorylation sites could be identified, suggesting the possibility of other kinases participating in the phosphorylation of these sites in vivo.

The phosphorylation sites of the α subunit are clustered in a region of only 80 amino acids, called multiphosphorylation segment[28]. This segment contains a large number of glycine and proline residues, making it a flexible structure (Supplementary Fig. 7a). As expected, the density for this loop was not visible in our cryo-EM structure in both states. The multiphosphorylation segment, adjacent to a predicted CaM binding region (residues 1046-1086), is thought to regulate the

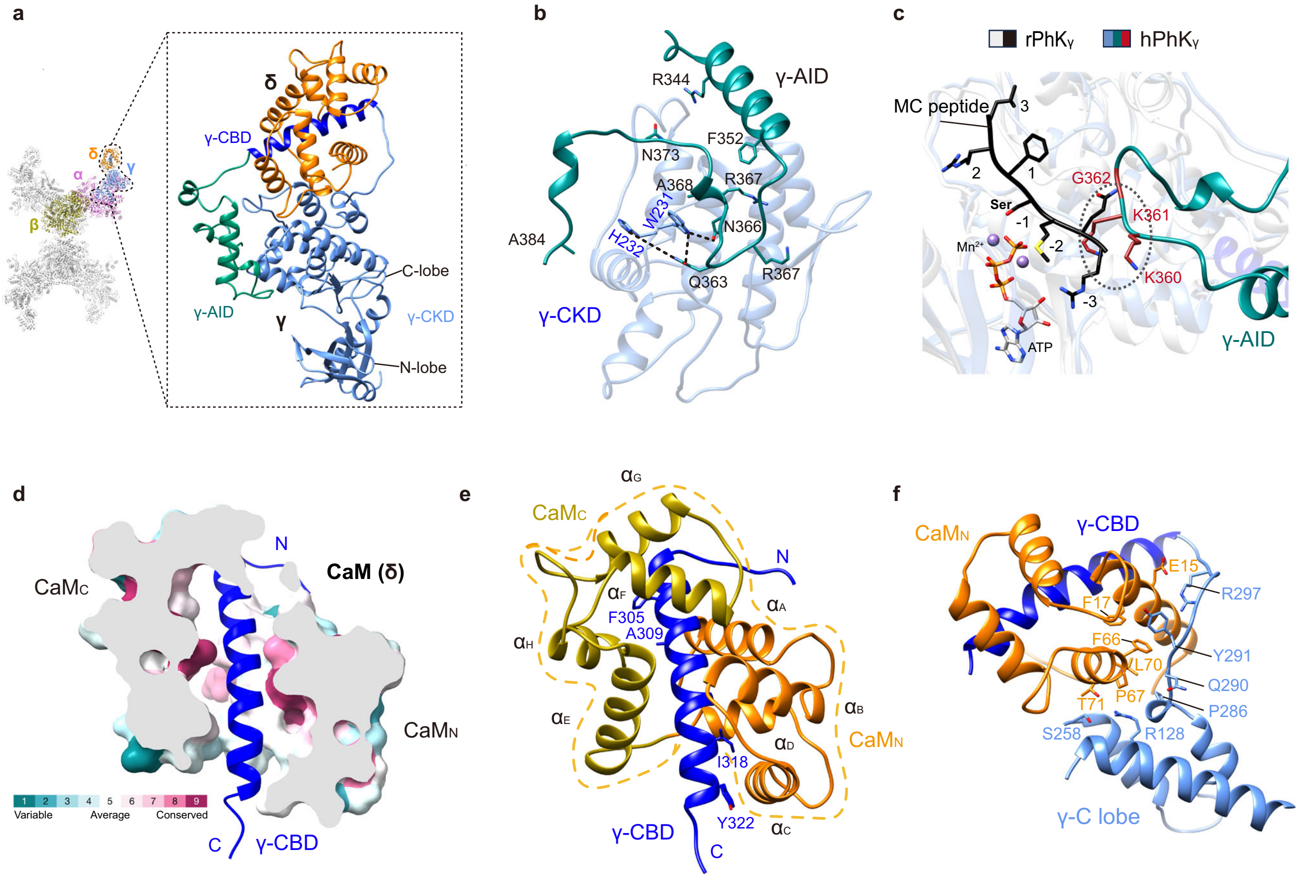

Fig. 2 | Structures and locations of γ and δ subunits. **a** Overall structure of the γδ complex. Left, the location of γ and δ subunits in one protomer of hPhK. Right, an enlarge view of the γδ complex. The γ-CKD, γ-CBD, and γ-AID regions are represented by cornflower blue, blue, and dark cyan, respectively, while the δ-subunit is represented by orange. The γ-CKD region consists of the N-lobe and C-lobe. **b** Interactions between the γ-AID region and γ-CKD region. Dotted lines correspond to putative hydrogen bonds. **c** Overlap the structure of CKD region of rPhK$_\gamma$ (PDB ID: 2PHK, with ATP and MC peptide) with hPhK$_\gamma$. G360, K361, and K362 from the AID region of hPhK$_\gamma$ conflict with the MC peptide. The hPhK$_\gamma$ is colored the same as (**a**), and the rPhK$_\gamma$ is colored by light gray and black. **d** Conserved surface mapping of δ subunit (CaM) using ConSurf. **e** Overall structure of CaM and γ-CBD region. **f** Interactions between CaM and C lobe of γ-CKD region.

activity of PhK by affecting the binding of exogenous CaM[29]. However, the phosphorylation of Ser1018$_\alpha$ is considered non-essential for activating PhK, merely serving to enhance the activating effect of the phosphorylated β subunit[30,31].

The phosphorylation sites of the β subunit are located in the N-terminus (Ser12 and Ser27, corresponding to Ser11 and Ser26 in the reference) and in the loop connecting the D2$_\beta$ and D3$_\beta$ regions (Ser701, corresponding to Ser700 in the reference), respectively[12,27]. The phosphorylation events make the loops that contain Ser26 and Ser700 detectable, playing a pivotal role in the phosphorylation-mediated regulation of PhK. This aspect will be further elaborated in subsequent sections. Furthermore, through tandem mass spectrometry (MS/MS) analysis, we have uncovered a number of previously unreported phosphorylation sites and mapped these sites onto the structural model (Supplementary Fig. 7b, c).

Regulation of hPhK by phosphorylation

The most fundamental way to activate hPhK is through phosphorylation and Ca^{2+}. The recombinant hPhK displays a partially phosphorylated state (Fig. 3c). To precisely investigate the regulatory effect of phosphorylation, hPhK underwent dephosphorylation and phosphorylation treatments utilizing Lambda-PP and PKAc, respectively (Fig. 3c). Similar to PhK purified from fast-twitch skeletal muscle of the rabbit[10], the recombinant hPhK also exhibits phosphorylation and Ca^{2+}-dependent activities, and this activity can be further enhanced at a pH of 8.2 (Fig. 3d).

This phosphorylated hPhK exhibits global structural changes compared to its unphosphorylated state, resulting in an outward rotation of each lobe along the tetramer axis (Supplementary Fig. 8a). Firstly, we analyzed the central bridges consisting of the β4 homotetramer. Notably, the structure analysis revealed a significant rotation of the phosphorylated β subunit, bringing it closer to the central core of the tetramer (Fig. 4a). Upon hPhK is phosphorylated, the distance between the joint of the bridge (β1 and β3 or β2 and β4) decreases by 1.6 Å, and the distance between the dimer of β subunits (β1 and β2 or β3 and β4) decreases by 4.2 Å (D2$_\beta$) or 7.1 Å (D5$_\beta$) (Fig. 4a). Since D5$_\beta$ functions as the junction of the central scaffold, it was selected for alignment to assess conformational changes within a single protomer (αβγδ). The D5$_\beta$ domain aligns well in two different states, with the remaining domains of the β subunit moving cohesively towards the D5$_\beta$. This coordinated movement also exerts a pull on the αγδ complex, drawing it in the same direction (Fig. 4b, c). The distances between the α and β subunits, the D2$_\alpha$ and γ-AID region, and the D5$_\alpha$ and γ-N lobe region have shortened by approximately 0.9 Å, 1.4 Å, and 0.3 Å, respectively (Supplementary Fig. 8b). After phosphorylation, the α subunit also undergoes conformational changes. When aligned with D1$_\alpha$, all the remaining domains within it will undergo slight movements towards D1$_\alpha$ (Supplementary Fig. 8c).

Compared to the inactive state, we observed two additional densities in the phosphorylated state: residues 13-42 (designated as Loop-27) and residues 675-710 (designated as Loop-701) in the β subunit (Supplementary Fig. 8d), which contain two crucial

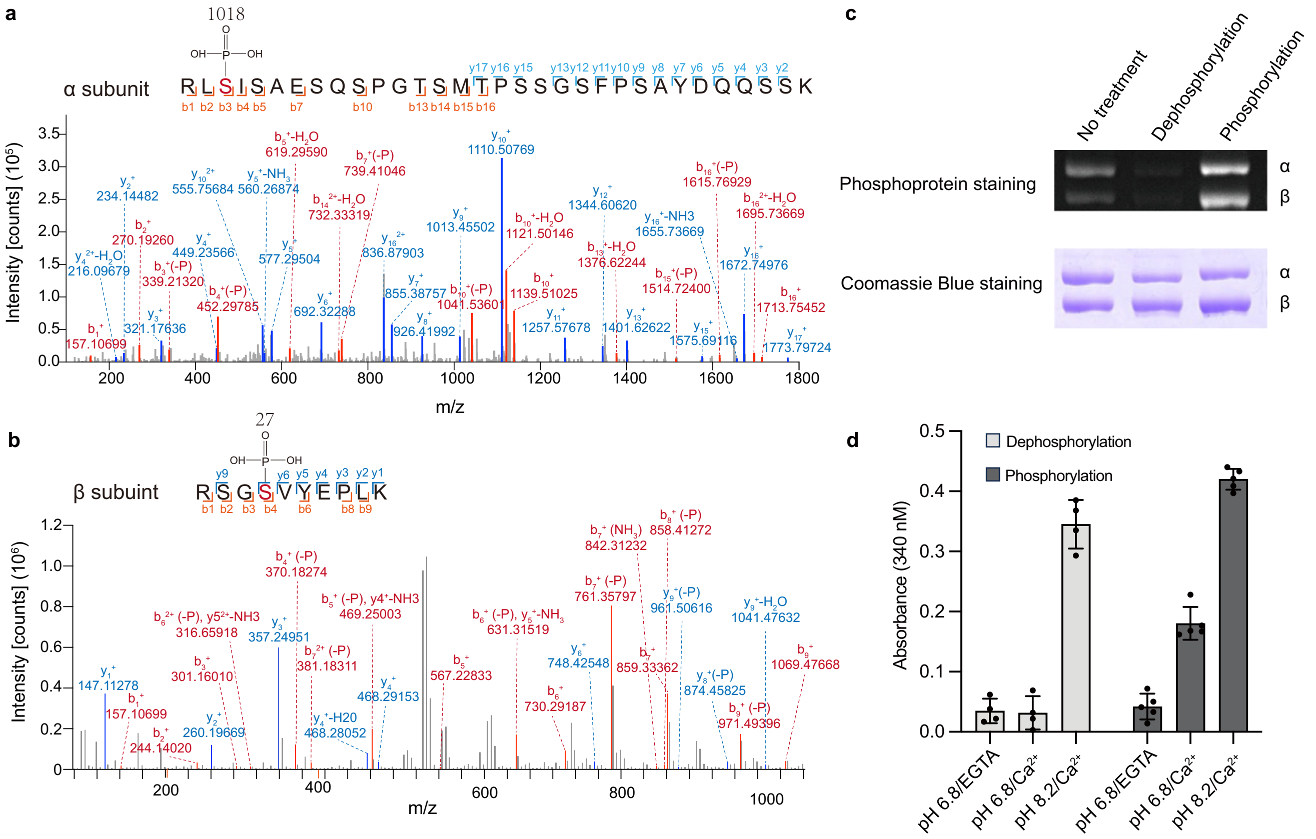

Fig. 3 | The phosphorylation of hPhK. a, b Representative annotated MS spectrum of the α (**a**) and β (**b**) subunits. **c** The phosphorylation level of hPhK. Phosphoprotein staining is used to detect phosphorylated proteins, while Coomassie Blue staining is used to detect total proteins. **d** The specific activities of dephosphorylated and phosphorylated hPhK at pH 6.8 and 8.2 in the presence of Ca^{2+} or EGTA. Data points represent the mean ± SD of four (Dephosphorylation) or five (phosphorylation) measurements.

phosphorylation sites, Ser27 and Ser701[12,27]. The Loop-27 has contact with $D1_β$, $D2_β$, and $D5_β$ of adjacent β subunit, bringing the β subunits (β1 and β2 or β3 and β4) into closer proximity (Fig. 4a, d). The Loop-701 connects $D2_β$ and $D3_β$ and is also located close to the N-lobe of the γ subunit (Fig. 4e). Additionally, $D2_β$ interacts with $D2_α$, and the movement of $D2_β$ causes the adjacent $D2_α$ to be pulled along (Supplementary Fig. 8b). Meanwhile, $D2_α$ engages with the N-lobe of the γ subunit, playing a pivotal role in maintaining the inactive state of the γ-subunit. Therefore, the conformational change of β subunit induced by phosphorylation may lead to the instability of the CKD region of the γ subunit, thereby facilitating the exposure of the catalytic center. To further explore these conformational changes between the inactive and phosphorylated states, Normal Mode Analysis (NMA) was performed to identify large-scale motions and dynamic coupling within the protein complex. The analysis revealed that while the β subunit remains highly stable, the other three subunits exhibit relatively large dynamics (Supplementary Fig. 9a, Supplementary Movie 1). In particular, the γ-AID and γ-CBD regions fluctuate in directions that form a specific angle, with γ-CBD showing a tendency to open upwards. This motion suggests a potential upward flipping movement in the γ-CKD region, which could further expose the catalytic center (Supplementary Figs. 9a, Supplementary Movie 2).

One ATP molecule was discovered in the cavity formed by $D1_β$, $D2_β$, and $D4_β$, and it forms two hydrogen bonds with $Arg214_β$ and $Pro798_β$, respectively (Figs. 4c and Supplementary Fig. 10a). ATP also serves as an allosteric regulator of PhK, and the conformational changes in the β subunit are the result of the combined action of phosphorylation and ATP. It is worth mentioning that previous reports suggested the presence of an ATP binding site in the α subunit, which was inferred by fluorescein 5′-isothiocyanate labeling, and that the binding of ATP to the α subunit would stimulate enzyme activity[27,32]. The α subunit and β subunit are highly homologous, sharing a sequence identity of up to 36.2%[33]. However, we did not find any additional density attributed to ATP at the identical site in the α subunit. It is possible that the amino acids stabilizing β-ATP subcomplex are not preserved in the α subunit, and that the amino acid $Lys49_α$, corresponding to $Pro798_β$, occupies the position for ATP entry (Supplementary Fig. 10b).

Regulation of hPhK by Ca^{2+}

After phosphorylation/Ca^{2+} activation, the γ-CBD region that binds with CaM becomes blurred. However, the conformation of the remaining region of the γ subunit undergoes almost no change (Fig. 5a). We also observed the binding of one ATP to the γ subunit of processed hPhK (Supplementary Fig. 10c). Although ATP is the essential phosphate donor for PhK catalysis, its binding did not alter the conformation of the γ subunit (Fig. 5a). After Ca^{2+} binding, we were able to observe the density of CaM at low resolution, but only one lobe of CaM could be fitted into the map (as depicted in Fig. 5b, where we have added the missing γ-CBD area for clarity). Compared with the γ-apo/CaM complex, the Ca^{2+} induced CaM moves along the γ-CBD helix toward γ-AID and α subunit (Fig. 5a). Usually, helices engage with Ca^{2+}/CaM through a set of 'aromatic anchor' residues[25,26]. The movement of Ca^{2+}/CaM may be achieved by strengthening the anchoring of $Tyr322_γ$ (Fig. 2e), analogous to the CaM/Myosin VIIa IQ motif complex[26], which leads to a decrease in the contact between CaM and the γ-C lobe. Furthermore, in the presence of Ca^{2+}, in vitro experiments indicate that exogenous CaM can enhance the activity of PhK through

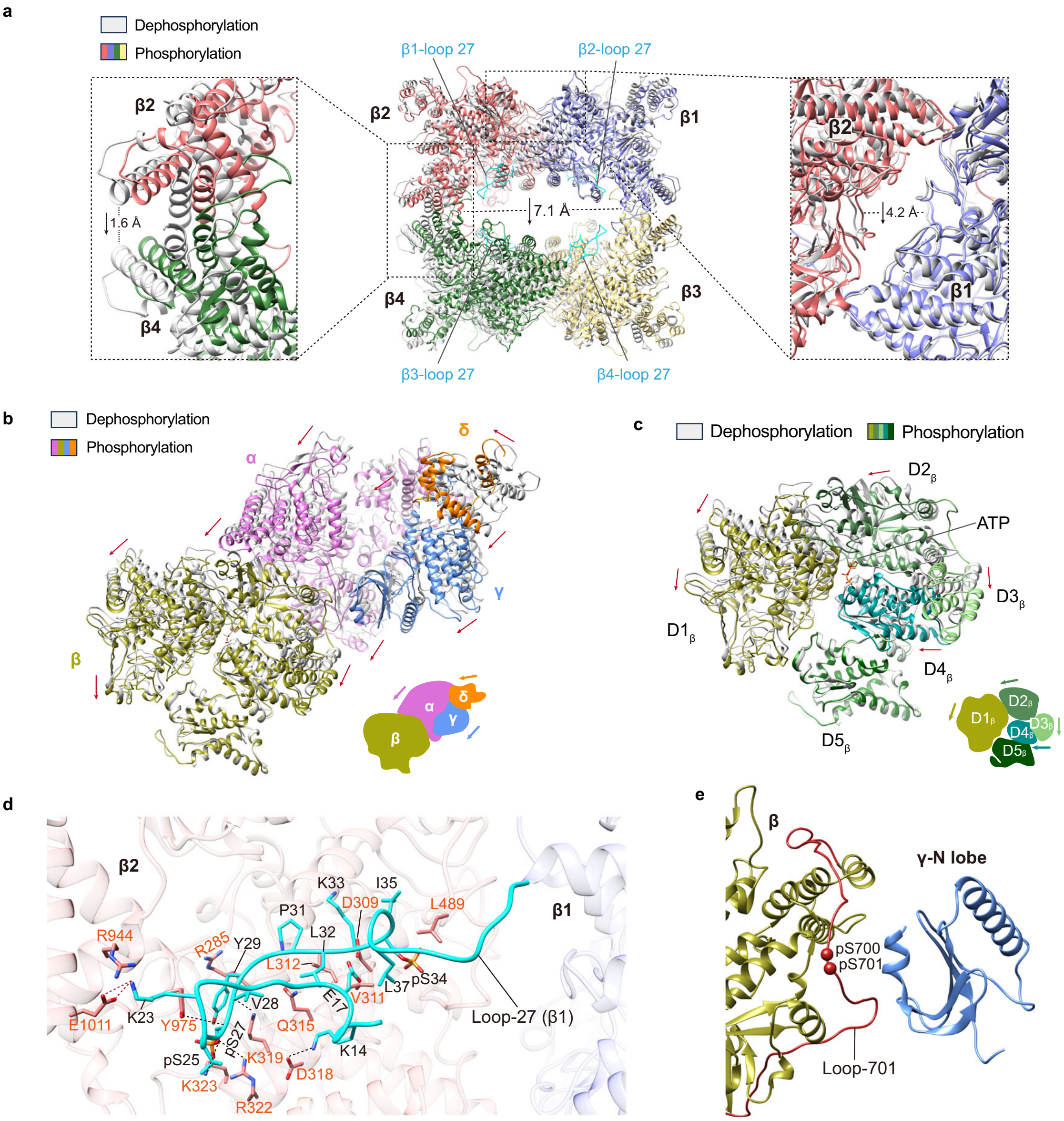

Fig. 4 | The conformational changes of hPhK after phosphorylation treatment. **a** Structural comparison of the central β_4 tetramer structure of dephosphorylated hPhK and phosphorylated hPhK. The left and right panels show the enlarged views of distance changes between β2/β4 and β1/β2, respectively. dephosphorylated hPhK is colored in light gray, while phosphorylated hPhK is colored according to Fig. 1a. The Loop-27 is depicted in cyan. **b** Structural comparison of dephosphorylated αβγδ subcomplex (light gray) and phosphorylated αβγδ subcomplex (colored). The red arrow indicates the direction of conformational change. The model in the lower right corner demonstrates the tendency of conformation changes. **c** Structural comparison of dephosphorylated β subunit (light gray) and phosphorylated β subunit (green). The red arrow indicates the direction of conformational change. The model in the lower right corner demonstrates the tendency of conformation changes. **d** Interaction details of the Loop-27 from β1 subunit and the adjacent β2 subunit. The β1 and β2 subunits are colored in slateblue and salmon, respectively, while Loop-27 is colored in cyan. Potential hydrogen bonds (black) and salt bridges (red) are indicated by dashed lines. **e** In the phosphorylated state, the β-subunit Loop-701 is located between the β subunit and the γ-N lobe. Phosphorylation sites are labeled by red balls.

interaction with both the α and β subunits[10,34]. Whether additional CaM regulation occurs in vivo requires further investigation.

NMA provided further insights into the dynamics of the CaM-γ complex. The analysis revealed that CaM exhibits a tendency to vibrate both toward γ-AID and upward. Notably, the vibrational directions of γ-AID and γ-CBD form relatively large angles with the vibrational direction of CaM (Supplementary Figs. 9a, Supplementary Movie 2). This angular divergence in the vibrational patterns likely facilitates the release of CaM's restraint on the γ-C lobe, thereby promoting the opening of the γ-CKD region. The vibrational motion observed in NMA also suggests that CaM movement is coupled with the upward motion of γ-CBD, which could serve as a trigger for conformational changes in the catalytic domain. This dynamic pattern may represent a mechanistic basis for the activation of PhK by Ca^{2+}/CaM, contributing to the exposure of the active site and enhancing enzymatic activity.

Comparison of hPhK under different activation conditions

Recent studies have reported on the structures of hPhK in both inactive and active conformational states[35]. Unlike to our method, their active state was achieved under alkaline conditions (pH 8.2) in the presence of Ca^{2+}. To better understand the regulatory effects of different activators on hPhK, we compared their activation states with ours. Since they did not observe the γ-CKD region and CaM under activation condition, our comparison primarily focused on the α and β subunits. At pH 8.2, the overall structure is closer to the central core of the tetramer compared to its phosphorylated state (Supplementary

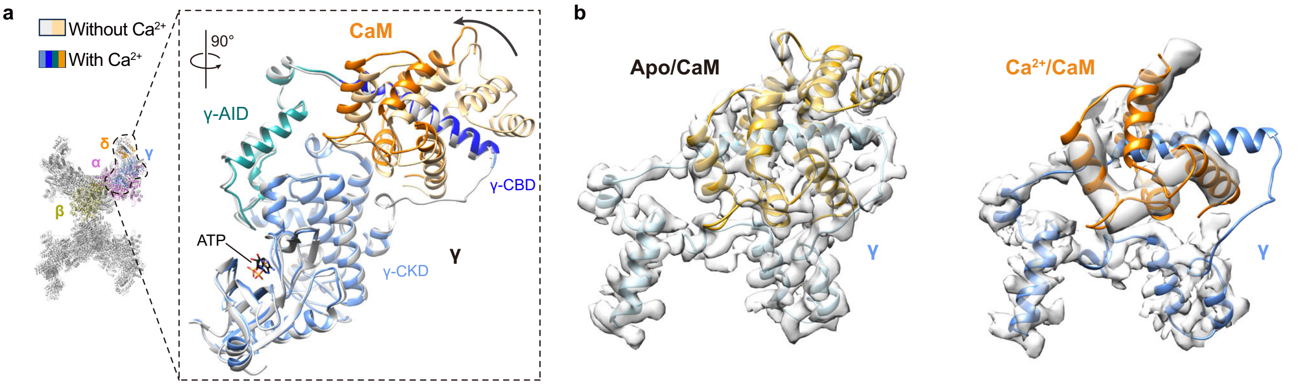

Fig. 5 | The regulation of hPhK by Ca^{2+}. **a** Structure overlay of the γ subunit and CaM (δ) complex in the apo state and the Ca^{2+} binding state. **b** EM map of the γ subunit and CaM in two states (left, without Ca^{2+}, right: with Ca^{2+}). In the presence of Ca^{2+}, only one lobe of CaM density is observable.

Fig. 11a). When comparing the central bridge specifically, which is composed of the β4 homotetramer, the distance between β4 units under different states follows this order: inactive > phosphorylated > pH 8.2 (Supplementary Fig. 11b). When aligning the αβ subcomplex with D5β for comparison, at a pH of 8.2, the α subunit moves towards the β subunit as a whole, resulting in a shortened distance between the two (Supplementary Fig. 11c). Additionally, the individual α subunit and β subunit also undergo a conformational rotation (Supplementary Figs. 11d, e). We previously introduced that after phosphorylation activation, hPhK exhibits a more compact structure compared to its inactive state (Supplementary Fig. 8a). Interestingly, at a pH of 8.2, hPhK further adopts an even more compact state relative to its phosphorylated structure. Prior research has suggested that the regulation of PhK activity by pH, to some extent, mimics other activation mechanisms[36,37]. Moreover, a pH of 8.2 can further augment activity under different activation conditions[10]. Therefore, we speculate that alkaline pH regulation of hPhK is similar to phosphorylation, but with a stronger activating effect.

Binding mode of PhK and GP

To gain insights into the mechanism of PhK catalyzing GP phosphorylation, we have tried a variety of methods to obtain the hPhK-GP complex, but none of them were successful. Eventually, we decided to employ XL-MS to investigate the interaction between hPhK and GP. In the non-active state, XL-MS analysis revealed that GP could covalently cross-link with the α and β subunits, respectively (Supplementary Fig. 12a). Specifically, Lys1042 from β1 and β4 or β2 and β3 subunits can precisely cross-link with the two monomers of GP, while Lys456 from α subunit can only bind with one monomer of GP (Supplementary Fig. 12b, c). Previous cross-linking experiment between GP and PhK, conducted under the condition of 20 mM HEPES (pH 6.8) and 0.1 mM EDTA using DFDNB, also indicated that GP directly interacts with the large regulatory α and β subunits of PhK[38]. This may represent a pre-binding state before GP binds to the γ subunit.

After activating hPhK through phosphorylation and Ca^{2+}, GP not only forms covalent cross-links with α and β subunits, but also with the γ subunit (Supplementary Fig. 12d). Under these conditions, we have found that one GP can simultaneously interact with both the α and β subunits (Lys793$_{GP}$/Lys302$_{\alpha}$ and Lys290$_{GP}$/Lys351$_{\beta}$). This may be due to the shortening of the distance between α and β subunits caused by phosphorylation, and it is speculated that this binding pattern facilitates the delivery of GP to the γ subunit (Supplementary Fig. 12e, f).

In addition, XL-MS revealed several cross-link sites between GP and the γ subunit (Supplementary Fig. 12d). By comprehensively considering the length of the cross-linking agent BS^3 and the spatial positions of PhK and GP, we speculated that the cross-link between Lys12 of GP and Lys143 of the γ subunit was relatively reasonable (Supplementary Fig. 12g). We employed a computationally modeled substrate loop of GP, given that the analogous segment in GPa is unable to fully extend into the catalytic cavity of the γ subunit. Upon phosphorylation from GPb to GPa, the substrate loop's conformation exhibits alterations, signifying the dynamic nature of this region throughout the phosphorylation event[39,40]. Consequently, we postulate that upon interaction with hPhK, the substrate loop will extend towards hPhK, representing an intermediate conformation between the two states of GP (Supplementary Fig. 12g).

To further validate the interaction between hPhK and GP, we utilized integrative structural modeling and molecular docking to obtain the complex structure of the activated hPhK tetramer bound to GP. The resulting model revealed the interaction between Lys12$_{GP}$ and Lys143$_{\gamma}$, which is consistent with our XL-MS findings. Further NMA of the complex indicated that both sides of the γ-CBD contain flexible loop regions, while the γ-CKD region exhibits a vibrational motion in the upward and downward directions (Supplementary Fig. 9b, Supplementary Movies 3-5). This dynamic behavior may explain why a stable conformation of the γ subunit cannot be captured at a pH of 8.2[35]. The downward motion of the γ-CKD region, as identified by NMA, likely enhances GP's interaction with the α and β subunits. This motion may account for the observed cross-links between GP and the regulatory subunits in the active state. Moreover, the γ subunit's inherent flexibility likely plays a crucial role in facilitating GP's transition from a pre-binding state to the active phosphorylation state, ensuring proper positioning of the substrate loop within the catalytic cavity for efficient phosphorylation.

Discussion

PhK, which was recognized by Krebs and Fischer 70 years ago[21], was the first protein kinase identified. It regulates glycogenolysis by integrating hormonal (cAMP and Ca^{2+}), neural (Ca^{2+}), and metabolic (ADP) signals, making it a central regulator in maintaining blood glucose homeostasis and energy supply[6,7]. The activation effect of cAMP is achieved through the phosphorylation of α and β subunits by PKA, while Ca^{2+} binds to the δ subunit (CaM) to exert its stimulatory effect. Our inactive hPhK cryo-EM structure indicates that hPhK is a hexadecamer composed of αβγδ tetramers, with the β subunit located at the center, the γδ subcomplex positioned at the edge, and the α subunit connecting in the middle (Fig. 1). Additionally, we also solved the structure of hPhK in phosphorylation/Ca^{2+} active state. Combined with XL-MS analysis of the interactions between hPhK and its substrate GP, our work provides a crucial framework for understanding the activation and catalysis of hPhK.

The activity of PhK is catalyzed by its γ subunit, and CaM functions as a structural component of PhK by stably associating with the γ-CBD region, even in the absence of Ca^{2+}[22]. Therefore, PhK is essentially a

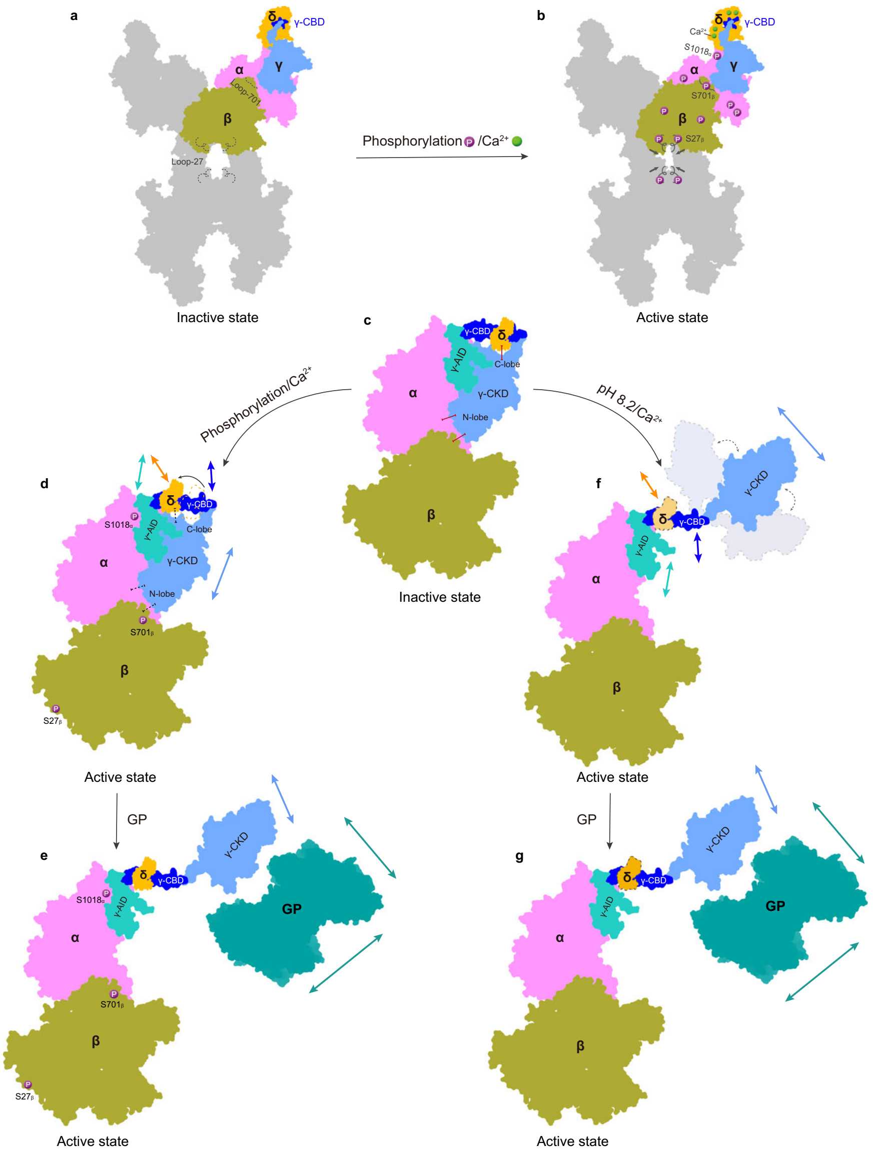

Fig. 6 | Proposed regulation model of hPhK activity. a, **b** and **c**–**g** show the regulation of holoenzyme and protomer, respectively. In the inactive state, the active sites of the γ-CKD region are occupied by the γ-AID region. Inactive hPhK can be activated in two ways: phosphorylation/Ca^{2+} or pH 8.2/Ca^{2+}. Phosphorylation primarily phosphorylates $Ser27_β$, $Ser701_β$, and $Ser1018_α$, resulting in the four protomers moving towards the center, thus disrupting the stability of the γ-N lobe. Ca^{2+} binds to the δ subunit (CaM), causing the δ subunit to slide along the γ-CBD region, which disrupts the stability of the γ-C lobe. The two processes work together to allow the γ-CKD region to flip when the substrate GP approaches, thus exposing the catalytic sites. pH 8.2/Ca^{2+} can keep the γ-CKD region in a flexible state, with the catalytic site exposed. When the substrate approaches, it can directly exert catalytic activity. Phosphorylation sites are shown as purple balls, and Ca^{2+} are shown as green balls. Only important phosphorylation sites are shown for simplicity. The red lines represent the lock between the γ subunit and the other three subunits, while the black lines indicate no lock. Arrows in corresponding colors represent the vibration directions of the respective subunits or domains.

Ca^{2+}/Calmodulin-dependent protein kinase (CaMK). Like other CaMKs, when Ca^{2+} is absent, the γ-AID region of hPhK occupies the substrate binding sites (Fig. 2c). However, PhK is distinct in that the inhibitory state of the γ subunit necessitates the collaborative action of the α, β, and δ subunits (Fig. 6a, c and Supplementary Fig. 6).

When the body's blood sugar concentration decreases or when a large amount of energy is required, the release of epinephrine and glucagon increases, which subsequently triggers the release of cAMP and Ca^{2+}. Subsequently, PKA phosphorylates the α and β subunits, and Ca^{2+} binds to CaM, which synergistically activates PhK. Based on our findings, we have formulated a model for PhK activation and its role in substrate phosphorylation (as depicted in Fig. 6). In the phosphorylation/Ca^{2+} active state, the phosphorylation of β subunits, particularly at the N-terminal $Ser27_β$, causes the four β subunits to cluster more closely, creating a more condensed central framework (Figs. 4 and 6d). This movement also draws D2α, affecting its interaction with the N-lobe of the γ-CKD region. Furthermore, phosphorylation at Ser701 of the β subunit diminishes the interaction between the N-lobe of the γ-CKD region and the remainder of PhK (Figs. 4 and 6d). Meanwhile, the phosphorylation of the α subunit reduces the distance to the γ-AID region, with the pivotal phosphorylation site $Ser1018_α$ in close proximity (Fig. 6b, d and Supplementary Fig. 8b). This promotes the γ subunit's continued attachment to the α subunit during catalytic activity. Additionally, our structural analysis indicates that Ca^{2+}/CaM moves along the γ-CBD region in relation to apo/CaM (Figs. 5a and 6d), a behavior that mirrors the observed interaction in the CaM/Myosin VIIa IQ motif complex[26]. This displacement may alleviate the constraint on the γ-C lobe of the γ-CKD region. The combined impact of phosphorylation and Ca^{2+} binding releases the constraints on the γ-CKD region, and the approach of the substrate GP triggers the swinging/

oscillation of the liberated γ-CKD region, thereby unveiling the catalytic site and enabling the phosphorylation process (Fig. 6e). The NMA results also illustrate the vibrational directions of individual domains within hPhK and reveal a tendency for the γ-CKD region to flip, facilitating the exposure of the catalytic center. These insights validate the feasibility of the large conformational changes proposed in our model (Supplementary Figs. 9 and Fig. 6d, e).

During the preparation of our manuscript, we became aware that Yang et al. also published the structures of PhK in both inactive and active conformations states[35]. The difference is that they achieved their active state under alkaline conditions (at a pH of 8.2) with the presence of Ca^{2+}. The electron densities for both the γ-CKD region and CaM in the active state were not observed. It was demonstrated that Ca^{2+} binding induces the dissociation of the γ-CKD region, thus relieving the inhibition of the kinase. An alkaline pH is considered to mimic the mechanisms of other activators, even though it can further enhance activity under varying activation conditions[10,36,37]. Therefore, we hypothesize that pH, acting as a potent activator, may collaborate with Ca^{2+} to maintain the γ-CKD in a dissociated state, facilitating substrate binding and consequently enhancing PhK activity (Fig. 6f, g).

PhK is acknowledged as one of the most intricately regulated kinases discovered to date. Beyond phosphorylation and Ca^{2+}, PhK activity is modulated by a variety of factors, Such as Mg^{2+}-ATP, glycogen, autophosphorylation, and other elements[22]. Evidence from various studies demonstrated that PhK undergoes dephosphorylation by a range of protein phosphatases, which underscores the complexity of its regulatory mechanisms[30]. Additionally, the apoptosis-related factor Caspase-3, which is associated with cancer progression, have been found to selectively cleave the regulatory α subunit of PhK, leading to its irreversible activation. This highlights the pivotal role of PhK activation in ATP production during programmed cell death and in the context of cancer growth[41,42]. Furthermore, although PhK is generally presumed to exist in equimolar ratios within the holoenzyme, it has been observed in some tumor tissues that the α and β subunits are overabundant compared to the γ subunit[18,19]. Therefore, the broader physiological functions of PhK, extending beyond its regulatory role over glycogen phosphorylase, deserve further investigation.

In conclusion, our study elucidates the regulation mechanism of phosphorylation and Ca^{2+} on the activity of PhK, and also clarifies the binding mode of PhK with its substrate under different states. Furthermore, our structures provide opportunities for the rational design of therapeutic molecules aimed at treating GSD IX and cancer.

Methods

Expression and purification of Lambda PP, PKA and CaM in *E. coli*

The gene encoding human serine/threonine-protein phosphatase (Lambda PP, UniProt ID: P03772) and human PKA catalytic domain (PKAc, UniProt ID: P17612) were cloned into the pET-28a vector with an N-terminal 6×His-tag, followed by an MBP fusion protein and a tobacco etch virus (TEV) protease cleavage site. Human Calmodulin (CaM, UniProt ID: P0DP25) was cloned into the pET-28a vector containing a 10×His-tag, an MsyB fusion protein and a TEV protease cleavage site at the N terminus. All three types of proteins were expressed and purified in the same manner. The plasmids were introduced into *Escherichia coli* BL21 (DE3) cells and grown at 37 °C in LB medium to OD600 ≈ 0.6-0.8. The cells were induced with 0.4 mM β-d-1-thiogalactopyranoside (IPTG) and grown at 18 °C overnight before harvesting.

After centrifugation at 7000 × *g* for 10 min, the cells were resuspended and sonicated in lysis buffer containing 20 mM HEPES pH 7.4, 250 mM NaCl, 10 mM 2-mercaptoethanol (*β*-ME), and 1 mM phenylmethanesulfonyl fluoride (PMSF). The cell debris was removed by centrifugation at 80,000 × *g* for 30 min, and the supernatant was loaded onto a pre-equilibrated HisTrap column (Cytiva). The column was washed with 10 column volumes (CV) of buffer A (10 mM HEPES pH 7.4, 250 mM NaCl), and eluted with 5 CV of buffer A plus 250 mM imidazole. The elute was cleaved with TEV protease overnight at 4 °C and simultaneously dialyzed against a buffer containing 10 mM Tris pH 8.0, and 100 mM NaCl. The proteins were further purified using an anion exchange column (ReSource Q, Cytiva) with a linear gradient from 100 to 700 mM NaCl in buffer B (10 mM Tris pH 8.0, 10 mM *β*-ME). The fractions of target protein were concentrated and injected onto a gel-filtration column (Superdex 200 10/300 GL, Cytiva), and eluted with buffer A. The peak fractions were collected, supplemented with 20% glycerol, and flash-frozen in liquid nitrogen before being stored at -80 °C.

Expression and purification of human PhK and GP in HEK293F cells

The genes encoding the full-length hPhK α-, β-, and γ-subunits, specifically PHKA1 (UniProt ID: P46020), PHKB (UniProt ID: Q93100), and PHKG1 (UniProt ID: Q16816), were cloned individually into the pCAG vector without any purification tags. Calmodulin, δ-subunit, was cloned into the pCAG vector containing an N-terminus Flag epitope tag. The gene encoding the full-length GP (PYGM, UniProt ID: P11217) was cloned into the pCAG vector with a C-terminus 10×His-tag and Flag epitope tag.

hPhK was expressed in HEK293F cells by transfecting with 2.25 mg plasmid (Equal amount for each subunit) and 4.5 mg of linear polyethylenimine (PEI) for 1 liter cells when the cell density reached ~2.5×10^6 cells/ml. After 12 h of transfection, 10 mM sodium butyrate was added to the culture medium to boost expression. The cells were further cultured for 48 h at 30 °C and harvested by centrifugation at 8000 × *g* for 10 min. The expression for GP was similar to that of hPhK, except for the amounts of plasmid and PEI used (1 mg plasmid, 3 mg PEI).

For the purification of hPhK, cells were resuspended in lysis buffer (50 mM HEPES pH 6.8, 200 mM NaCl, 4 mM EDTA, 1% triton, 10% glycerol, 1 mM Dithiothreitol (DTT), EDTA-free protease inhibitor cocktail (MedChemExpress)) and gently stirred for 1 h at 4 °C. After centrifugation at 80,000 × *g*, the supernatant was collected and applied to anti-Flag M2 affinity resin. The resin was rinsed with buffer C (25 mM HEPES pH 6.8, 150 mM NaCl, 2 mM EDTA, 1 mM DTT) and eluted with buffer C supplemented with 200 μg/ml FLAG peptide. Concentrated hPhK proteins from affinity resin were dephosphorylated and phosphorylated by Lambda PP and PKAc in a molar ratio of 1:1 at 30 °C for 1 h, respectively. The phosphorylation level of hPhK was determined using Diamond Phosphoprotein Gel Stain (Invitrogen). The dephosphorylated and phosphorylated hPhK were further purified using the size-exclusion chromatography (Superose 6 10/300 GL, Cytiva), respectively.

For the purification of GP, the collected cells were resuspended in lysis buffer (50 mM Tris, pH 7.4, 200 mM NaCl, 1% Triton X-100, 10% glycerol, 1 mM DTT, EDTA-free protease inhibitor cocktail) for 1 h at 4 °C. The cell debris was removed by centrifugation at 80,000 × *g* for 1 h. The supernatant was incubated with anti-Flag M2 affinity resin and eluted by buffer A supplemented with 200 μg/ml FLAG peptide and 1 mM DTT. The protein eluent was concentrated and run over a Superdex 200 10/300 gel filtration column (Cytiva) in buffer A plus 1 mM DTT.

Kinase activity assays

The conversion of GPb to GPa by hPhK was performed following a protocol modified from previously described methods[22]. The reaction buffer for the conversion comprised 50 mM HEPES, 2 mM DTT, 1 mM ATP, 10 mM $Mg(CH_3CO_2)_2$, 0.5 mg/ml bovine serum albumin, 1 mg/ml GPb, and 1 mM EGTA or 0.5 mM $CaCl_2$. The final pH of the reactions was 8.2 or 6.8. The reactions were carried out at 30 °C and initiated with the addition of PhK (80 ng/ml) after preincubating the other components for 2 min. After 5 min, the reactions were terminated by the addition of 5 times ice-cold buffer containing 100 mM Tris pH 6.8, 1 mM EDTA, 2 mM DTT.

GPa was measured using the Glycogen Phosphorylase a (GPa) Activity Assay Kit (Solarbio Life Science). GPa catalyzes the production of glucose residues from glycogen and inorganic phosphorus to glycogen and glucose 1-phosphate. Under the action of phosphoglucose mutase and glucose-6-phosphate dehydrogenas, it further catalyzes the reduction of $NADP^+$ to NADPH. According to the manufacturer's instruction, 10 µl product from the last step was added to a 200 µl reaction volume and the increase of NADPH was recorded from the microplate wells at 340 nm.

Cryo-EM sample preparation and data acquisition

To prepare the inactive state hPhK, dephosphorylated hPhK was applied to size-exclusion chromatography (Superose 6 10/300 GL, Cytiva) and eluted with a buffer containing 25 mM HEPES pH 6.8, 150 mM NaCl, 5 mM EGTA, and 1 mM DTT. For the preparation of the activated state of hPhK, the phosphorylated hPhK was loaded onto the same size-exclusion chromatography and eluted with a buffer containing 25 mM HEPES pH 6.8, 150 mM NaCl, 1 mM $CaCl_2$, 5 mM $MgCl_2$, and 1 mM DTT. Prior to the preparation of cryo-EM samples, CaM was added to both states of hPhK at a molar ratio of 4:1, and a final concentration of 4 mM ATP was additionally added to the activated hPhK. The protein concentration used for cryo-EM sample preparation was ~2.5 mg/ml. Before sample vitrification, hPhK was supplemented with DDM to a final concentration of 0.01% to prevent the protein from denaturing at the air-water interface. Aliquots of 3 µl hPhK protein samples were applied to holy grids (Cu R1.2/1.3, 300 mesh, Quantifoil) glow discharged by PELCO easiGlow. The grids were blotted for 4 s at 5 °C and 100% humidity using a FEI Vitrobot Mark IV (Thermo Fisher Scientific). The inactive hPhK sample was also prepared using continuous carbon-coated grids (Cu R1.2/1.3 + 2 nM C, 300 mesh, Quantifoil)) in 1 mg/ml without DDM and blotted for 0.5 s.

The grids of inactive hPhK were transferred to a Titan Krios G3 electron microscope (Thermo Fisher Scientific) equipped with a Gatan Quantum Energy Filter (GIF, slit width of 20 eV) and a Falcon 4 detector (Thermo Fisher Scientific), operating at 300 kV in the super-resolution mode. Images were obtained with a magnification of 75,000×, corresponding to a physical pixel size of 1.1 Å. Defocus ranged from -2.0 to -1.0 µm, with a total dose of 50 e^- $Å^{-2}$ applied equally for 32 frames. In total 3,635 and 4,570 movies were collected for Cu grid and carbon-coated grid, respectively. A total of 3,848 movies of active hPhK were collected on a Titan Krios G3i electron microscope (Thermo Fisher Scientific) equipped with a Gatan Quantum Energy Filter (GIF, slit width of 20 eV) and a Gatan K3 Summit direct electron detector in the super-resolution mode. All the other values were the same as above, except for a magnification of 81,000× in super-resolution mode, resulting in a pixel size of 0.547 Å.

Data processing

Data processing procedures were summarized in flow charts in the Supplementary Table 1. All movie stacks were corrected for beam-induced motion correction using MotionCor2[43] and estimated the contrast transfer function (CTF) using CTF estimation (Gctf) in cryoSPARC[44]. Subsequently, hundreds of micrographs were selected for automatic particle picking using the Blob picker and subjected to 2D classification analysis. The result of 2D classification was used as templates. Good particles were selected as templates for picking particles from the remaining micrographs. All particles were extracted with a box size of 480 pixels and were used for 2D classification. After multiple rounds of 2D classification, the selected particles were used for Ab-initio reconstruction to generate initial maps in cryoSPARC. Particles from initial model classes with good integrity were subjected to further heterogeneous refinement and non-uniform refinement, resulting in the generation of the final map. Local refinement was used to improve the quality of local density map. The overall resolution of the final map was estimated using the gold-standard Fourier shell correlation at 0.143 criterion. The local resolution maps were evaluated using Local Resolution Estimation in cryoSPARC[44].

Model building and refinement

The preliminary models of α, β, and γ subunits of PhK were generated by AlphaFold[45] and a preliminary model of CaM was from the crystal structure of Ca^{2+}/CaM (PDB: 2WEL). These preliminary models were first rigid body fitted into the cryo-EM density maps using UCSF Chimera[46], respectively. Subsequent model adjustments and rebuilding were done with Coot[47]. Structure refinement was carried out using PHENIX real-space refine[48].

Liquid chromatography with tandem mass spectrometry (LC-MS/MS) analysis

Phosphorylated PhK proteins were first reduced and alkylated, and then digested with trypsin (Promega) in solution. The peptides were loaded to an analytical column (100 µm i.d × 20 cm) packed with 1.9 µm and 120 Å ReproSil-Pur C18 resins (Dr. Maisch GmbH, Ammerbuch, Germany). Mobile phase A consisted of 0.1% formic acid (FA) in water, and mobile phase B consisted of 0.1% FA in acetonitrile (ACN). Gradients were run from 7% to 22% mobile phase B for 50 min followed by 22%-35% mobile phase B for 10 min. The full mass scan was acquired from m/z 350 to 1550 with resolution 120,000 at a target of 2e5 ions, and the MS/MS spectra were obtained in a data dependent acquisition in the top speed mode with higher-energy collision dissociation (target 5e4 ions, max ion injection time 40 ms, isolation window 1.6 m/z, normalized collision energy 30%). The dynamic exclusion time was set to 30 s. Precursor ions with unassigned charge state as well as charge state of 1+ or superior to 6+ were excluded from fragmentation.

The LC-MS/MS data were subsequently analyzed by searching against the UniProt-Homo sapiens database utilizing Proteome Discoverer 2.4.1.15 (Thermo). The search parameters were set with a mass tolerance of 10 ppm for the first-order mass spectrum and 0.02 Da for the second-order mass spectrum. During the enzymatic digestion process, a maximum of 2 missed cleavages were permitted, and the peptide lengths ranged from 4 to 144 amino acids. The carbamidomethylation of cysteine (C) was considered as a fixed modification, while the variable modifications encompassed oxidation of methionine (M), phosphorylation of serine, threonine, or tyrosine (S/T/Y), and farnesylation on the C-terminal cysteine (C). The experiment was repeated three times, and the phosphorylation sites that were present in all three trials were selected for subsequent analysis.

Cross-linking mass spectrometry (XL-MS) analysis

The hPhK proteins (1 µM) in both inactive and active states were premixed with GP at a molar ratio of 1:1.5 and cross-linked by 2 mM BS^3 (bis[sulfosuccinimidyl] suberate; Thermo Scientific) at 25 °C for ~30 min. The reaction solutions were precipitated using acetone and then resuspended in a solution containing 8 M urea and 100 mM Tris-HCl pH 8.5. Subsequently, the samples underwent reduction and alkylation processes using TCEP and iodoacetamide, respectively. Following overnight digestion with trypsin (Promega) at a ratio of 1:50 (w/w), the resulting peptide solutions were desalted using a MonoSpin™ C18 column (GL Science, Tokyo, Japan) and subsequently dried using a SpeedVac.

The peptide mixture was analyzed by an Easy-nLC 1200 nano HPLC (Thermo Scientific, San Jose, CA) using a customized 30 cm-long pulled-tip analytical column (75 µm ID packed with ReproSil-Pur C18-AQ 1.9 µm resin, Dr. Maisch GmbH, Germany) at 55 °C. A binary mobile phase system was used, with the first one remaining as mobile phase A: 0.1% FA in water, and the second one, mobile phase C, consisting of 0.1% FA in 80% ACN. The gradients were as follows: 0-1 min, 6%-10% B; 1-96 min, 10-36% B; 96-107 min, 36%-60% B, 107-108 min, 60%-100% B, 108-120 min, 100% B. The flow rate was set as 300 nl/min.

Peptides eluted from the LC column were directly electrosprayed into the Q Exactive Orbitrap mass spectrometer (Thermo Scientific, San Jose, CA) with the application of a distal 2.2 kV spray voltage. A cycle of one full-scan MS spectrum (m/z 300-1800) was acquired followed by top 20 MS/MS events, sequentially generated on the first to the twentieth most intense ions selected from the full MS spectrum at a 28% normalized collision energy. Full scan resolution was set to 70,000 with automated gain control (AGC) target of 3e6. MS/MS scan resolution was set to 17,500 with isolation window of 1.8 m/z and AGC target of 1e5. The number of microscans was one for both MS and MS/MS scans and the maximum ion injection time was 50 and 100 ms, respectively. The dynamic exclusion settings used were as follows: charge exclusion, 1, 2 and >8; exclude isotopes, on; and exclusion duration, 5, 10 or 15 sec. MS scan functions and LC solvent gradients were controlled by the Xcalibur data system (Thermo Scientific).

Peptides containing the isopeptide bonds were identified using pLink2 software (pFind Team, Beijing, China), with the human PhK protein serving as the database[49,50]. The search parameters in pLink were set as follows: a maximum of three missed cleavages were allowed; the peptide length ranged from 6 to 60 amino acids, with a peptide mass per chain ranging from a minimum of 600 Da to a maximum of 6000 Da. Both the precursor and fragment mass tolerances were set to 20 ppm. The cross-linker BS3 (cross-linking sites: Lysine and protein N-terminus) has a mass shift of 138.06808 Da for the light cross-linker and a mass shift of 156.0786 Da for mono-links. Carbamidomethylation of cysteine and oxidation of methionine were specified as the fixed modification and the variable modification, respectively. Subsequently, the results were filtered by applying a 5% false discovery rate (FDR) cutoff at the spectral level.

Normal mode analysis (NMA) and integrative structural modeling

The activated structure of the hPhK was used for NMA study. In this analysis, the anisotropic network model (ANM)[51,52] was employed as the elastic network model, using Cα atoms from the structure to construct the Hessian matrix. This matrix was then diagonalized to calculate the frequencies and modes of each order. Protein structural dynamics were analyzed using the open-source Python package ProDy[53], with a cutoff parameter set to 15.0 and gamma set to 1.0. The analysis yielded the first 20 non-zero modes for both the monomer and tetramer structures, with the top 3 modes visualized using the Normal Mode Wizard plugin in VMD[54] (version 1.9.3) and animated using FFmpeg (https://www.ffmpeg.org/).

Next, we extended the NMA analysis to the GP-bound activated structure of the PhK tetramer. To construct this complex model, we developed an integrative structural modeling protocol by combining AlphaFold structure predictions, molecular docking, and cross-linking mass spectrometry (XL-MS) data. The open conformation of the γ domain was achieved by manually adjusting the γ-CKD domain using PyMOL, while the missing loop regions were modeled using GalaxyFill[55]. The structure of the human GP dimer (muscle form) was predicted using the AlphaFold3 web server[56]. The complex structure of the GP dimer and PhK was modeled using HADDOCK2.4[57] with the binding interface between GP and the γ domain of PhK constrained by the cross-linking mass spectrometry data. The constructed hPhK-GP model was subsequently subjected to NMA using the same ANM-based parameters as those used for the analysis of the activated hPhK structure.

Reporting summary

Further information on research design is available in the Nature Portfolio Reporting Summary linked to this article.

Data availability

Atomic coordinates of hPhK have been deposited in the PDB (http://www.rcsb.org/) under the accession codes 8Z5Q (inactive, tetramer), 8Z5P (inactive, dimer), 8Z5M (inactive, αγδ subcomplex), 8Z5T (active, tetramer), and 8Z5R (active, αγδ subcomplex), respectively. The corresponding EM maps have been deposited in the Electron Microscopy Data Bank (https://www.ebi.ac.uk/pdbe/emdb/), under the accession codes EMD-39778 (inactive, tetramer), EMD-39777 (inactive, dimer), EMD-39775 (inactive, αγδ subcomplex), EMD-39784 (inactive, protomer), EMD-39781 (active, tetramer), EMD-39779 (active, αγδ subcomplex), and EMD-39785 (active, protomer) respectively. The mass spectrometry proteomics data have been deposited to the ProteomeXchange Consortium (http://proteomecentral.proteomexchange.org) via the PRIDE partner repository with the dataset identifier PXD059345 (phosphorylation modification), PXD059356 (XL-MS in inactive state), and PXD059369 (XL-MS in active state). Source data are provided with this paper.

References

1. Roach, P. J., Depaoli-Roach, A. A., Hurley, T. D. & Tagliabracci, V. S. Glycogen and its metabolism: some new developments and old themes. *Biochem J.* **441**, 763–787 (2012).
2. Rimmer, M. A., Nadeau, O. W., Artigues, A. & Carlson, G. M. Structural characterization of the catalytic gamma and regulatory beta subunits of phosphorylase kinase in the context of the hexadecameric enzyme complex. *Protein Sci.* **27**, 485–497 (2018).
3. Sprang, S. R., Withers, S. G., Goldsmith, E. J., Fletterick, R. J. & Madsen, N. B. Structural basis for the activation of glycogen phosphorylase b by adenosine monophosphate. *Science* **254**, 1367–1371 (1991).
4. Brushia, R. J. & Walsh, D. A. Phosphorylase kinase: the complexity of its regulation is reflected in the complexity of its structure. *Front Biosci.* **4**, D618–D641 (1999).
5. Vénien-Bryan, C. et al. Three-dimensional structure of phosphorylase kinase at 22 Å and its complex with glycogen phosphorylase b. *Structure* **10**, 33–41 (2002).
6. Yeaman, S. J. & Cohen, P. The hormonal control of activity of skeletal muscle phosphorylase kinase. phosphorylation of the enzyme at two sites in vivo in response to adrenalin. *Eur. J. Biochem.* **51**, 93–104 (1975).
7. Paudel, H. K. & Carlson, G. M. Inhibition of the catalytic subunit of phosphorylase kinase by its alpha/beta subunits. *J. Biol. Chem.* **262**, 11912–11915 (1987).
8. Ozawa, E. Activation of phosphorylase kinase from brain by small amounts of calcium ion. *J. Neurochem.* **20**, 1487–1488 (1973).
9. Cohen, P. et al. Identification of the Ca2+-dependent modulator protein as the fourth subunit of rabbit skeletal muscle phosphorylase kinase. *FEBS Lett.* **92**, 287–293 (1978).
10. Cohen, P. The role of calcium ions, calmodulin and troponin in the regulation of phosphorylase kinase from rabbit skeletal muscle. *Eur. J. Biochem* **111**, 563–574 (1980).
11. Newsholme, P. & Walsh, D. A. A kinetic re-interpretation of the regulation of rabbit skeletal-muscle phosphorylase kinase activity by Ca2+ and phosphorylation. *Biochem J.* **283**, 845–848 (1992).
12. Andreeva, I. E., Makeeva, V. F., Livanova, N. B., Petukhov, S. P. & Kurganov, B. I. Studies on interaction of phosphorylase kinase from rabbit skeletal muscle with glycogen in the presence of ATP and ADP. *Biochim Biophys. Acta* **1549**, 188–196 (2001).
13. Cheng, A., Fitzgerald, T. J. & Carlson, G. M. Adenosine 5′-diphosphate as an allosteric effector of phosphorylase kinase from rabbit skeletal muscle. *J. Biol. Chem.* **260**, 2535–2542 (1985).
14. Nadeau, O. W., Fontes, J. D. & Carlson, G. M. The regulation of glycogenolysis in the brain. *J. Biol. Chem.* **293**, 7099–7107 (2018).
15. Bali, D. S. et al. Clinical and molecular variability in patients with PHKA2 variants and liver phosphorylase b kinase deficiency. *JIMD Rep.* **37**, 63–72 (2017).
16. Ellingwood, S. S. & Cheng, A. Biochemical and clinical aspects of glycogen storage diseases. *J. Endocrinol.* **238**, R131–R141 (2018).

17. Akman, H. O. et al. Fatal infantile cardiac glycogenosis with phosphorylase kinase deficiency and a mutation in the gamma2-subunit of AMP-activated protein kinase. *Pediatr. Res* **62**, 499–504 (2007).
18. Camus, S. et al. Identification of phosphorylase kinase as a novel therapeutic target through high-throughput screening for anti-angiogenesis compounds in zebrafish. *Oncogene* **31**, 4333–4342 (2012).
19. Wang, G. et al. Phosphorylase kinase beta affects colorectal cancer cell growth and represents a novel prognostic biomarker. *J. Cancer Res. Clin.* **143**, 971–980 (2017).
20. Yang, W. et al. Phosphorylase kinase beta represents a novel prognostic biomarker and Inhibits malignant phenotypes of liver cancer cell. *Int J. Biol. Sci.* **15**, 2596–2606 (2019).
21. Fischer, E. H. & Krebs, E. G. Conversion of phosphorylase b to phosphorylase a in muscle extracts. *J. Biol. Chem.* **216**, 121–132 (1955).
22. Venien-Bryan, C. et al. The structure of phosphorylase kinase holoenzyme at 9.9 angstroms resolution and location of the catalytic subunit and the substrate glycogen phosphorylase. *Structure* **17**, 117–127 (2009).
23. Nadeau, O. W. et al. Structure and location of the regulatory beta subunits in the (alphabetagammadelta)4 phosphorylase kinase complex. *J. Bio Chem.* **287**, 36651–36661 (2012).
24. Lowe, E. D. et al. The crystal structure of a phosphorylase kinase peptide substrate complex: kinase substrate recognition. *EMBO J.* **16**, 6646–6658 (1997).
25. Van Petegem, F., Chatelain, F. C. & Minor, D. L. Jr Insights into voltage-gated calcium channel regulation from the structure of the CaV1.2 IQ domain-Ca2+/calmodulin complex. *Nat. Struct. Mol. Biol.* **12**, 1108–1115 (2005).
26. Li, J. et al. Ca2+-induced rigidity change of the myosin VIIa IQ motif-single alpha helix lever arm extension. *Structure* **25**, 579–591.e574 (2017).
27. Heilmeyer, L. M. Jr Molecular basis of signal integration in phosphorylase kinase. *Biochim Biophys. Acta* **1094**, 168–174 (1991).
28. Wüllrich, A., Hamacher, C., Schneider, A. & Kilimann, M. The multiphosphorylation domain of the phosphorylase kinase alpha M and alpha L subunits is a hotspot of differential mRNA processing and of molecular evolution. *J. Biol. Chem.* **268**, 23208–23214 (1993).
29. Meyer, H. E., Meyer, G. F., Dirks, H. & Heilmeyer, L. M. Jr Localization of phosphoserine residues in the alpha subunit of rabbit skeletal muscle phosphorylase kinase. *Eur. J. Biochem* **188**, 367–376 (1990).
30. Ramachandran, C., Goris, J., Waelkens, E., Merlevede, W. & Walsh, D. The interrelationship between cAMP-dependent alpha and beta subunit phosphorylation in the regulation of phosphorylase kinase activity. Studies using subunit specific phosphatases. *J. Biol. Chem.* **262**, 3210–3218 (1987).
31. Pickett-Gies, C. & Walsh, D. Subunit phosphorylation and activation of skeletal muscle phosphorylase kinase by the cAMP-dependent protein kinase. Divalent metal ion, ATP, and protein concentration dependence. *J. Biol. Chem.* **260**, 2046–2056 (1985).
32. Zaman, N. et al. Reaction of fluorescein isothiocyanate with an ATP-binding site on the phosphorylase kinase alpha subunit. *Eur. J. Biochem* **182**, 577–584 (1989).
33. Kilimann, M. W. et al. The alpha and beta subunits of phosphorylase kinase are homologous: cDNA cloning and primary structure of the beta subunit. *Proc. Natl Acad. Sci. USA* **85**, 9381–9385 (1988).
34. Shenolikar, S., Cohen, P. T., Cohen, P., Nairn, A. C. & Perry, S. V. The role of calmodulin in the structure and regulation of phosphorylase kinase from rabbit skeletal muscle. *Eur. J. Biochem* **100**, 329–337 (1979).
35. Yang, X., Zhu, M., Lu, X., Wang, Y. & Xiao, J. Architecture and activation of human muscle phosphorylase kinase. *Nat. Commun.* **15**, 2719 (2024).
36. Newsholme, P., Angelos, K. L. & Walsh, D. A. High and intermediate affinity calmodulin binding domains of the alpha and beta subunits of phosphorylase kinase and their potential role in phosphorylation-dependent activation of the holoenzyme. *J. Biol. Chem.* **267**, 810–818 (1992).
37. Chan, K. F. & Graves, D. J. Isolation and physicochemical properties of active complexes of rabbit muscle phosphorylase kinase. *J. Biol. Chem.* **257**, 5939–5947 (1982).
38. Thompson, J. A. & Carlson, G. M. The regulatory alpha and beta subunits of phosphorylase kinase directly interact with its substrate, glycogen phosphorylase. *Biochem Biophys. Res Commun.* **482**, 221–225 (2017).
39. Barford, D., Hu, S. H. & Johnson, L. N. Structural mechanism for glycogen phosphorylase control by phosphorylation and AMP. *J. Mol. Biol.* **218**, 233–260 (1991).
40. Owen, D. J., Noble, M. E., Garman, E. F., Papageorgiou, A. C. & Johnson, L. N. Two structures of the catalytic domain of phosphorylase kinase: an active protein kinase complexed with substrate analogue and product. *Structure* **3**, 467–482 (1995).
41. Hilder, T. L., Carlson, G. M., Haystead, T. A., Krebs, E. G. & Graves, L. M. Caspase−3 dependent cleavage and activation of skeletal muscle phosphorylase b kinase. *Mol. Cell Biochem* **275**, 233–242 (2005).
42. Liu, X. et al. Caspase-3 promotes genetic instability and carcinogenesis. *Mol. Cell* **58**, 284–296 (2015).
43. Zheng, S. Q. et al. MotionCor2: anisotropic correction of beam-induced motion for improved cryo-electron microscopy. *Nat. Methods* **14**, 331–332 (2017).
44. Punjani, A., Rubinstein, J. L., Fleet, D. J. & Brubaker, M. A. cryoSPARC: algorithms for rapid unsupervised cryo-EM structure determination. *Nat. Methods* **14**, 290–296 (2017).
45. Tunyasuvunakool, K. et al. Highly accurate protein structure prediction for the human proteome. *Nature* **596**, 590–596 (2021).
46. Goddard, T. D. et al. UCSF ChimeraX: meeting modern challenges in visualization and analysis. *Protein Sci.* **27**, 14–25 (2018).
47. Emsley, P. & Cowtan, K. Coot: model-building tools for molecular graphics. *Acta Crystallogr D. Biol. Crystallogr* **60**, 2126–2132 (2004).
48. Adams, P. D. et al. PHENIX: a comprehensive Python-based system for macromolecular structure solution. *Acta Crystallogr D. Biol. Crystallogr* **66**, 213–221 (2010).
49. Lu, S. et al. Mapping native disulfide bonds at a proteome scale. *Nat. Methods* **12**, 329–331 (2015).
50. Yang, B. et al. Identification of cross-linked peptides from complex samples. *Nat. Methods* **9**, 904–906 (2012).
51. Atilgan, A. R. et al. Anisotropy of fluctuation dynamics of proteins with an elastic network model. *Biophys. J.* **80**, 505–515 (2001).
52. Doruker, P., Atilgan, A. R. & Bahar, I. Dynamics of proteins predicted by molecular dynamics simulations and analytical approaches: application to alpha-amylase inhibitor. *Proteins* **40**, 512–524 (2000).
53. Bakan, A., Meireles, L. M. & Bahar, I. ProDy: protein dynamics inferred from theory and experiments. *Bioinformatics* **27**, 1575–1577 (2011).
54. Humphrey, W., Dalke, A. & Schulten, K. VMD: visual molecular dynamics. *J. Mol. Graph* **14**, 33–38 (1996). 27-38.
55. Coutsias, E. A., Seok, C., Jacobson, M. P. & Dill, K. A. A kinematic view of loop closure. *J. Comput Chem.* **25**, 510–528 (2004).
56. Abramson, J. et al. Accurate structure prediction of biomolecular interactions with AlphaFold 3. *Nature* **630**, 493–500 (2024).
57. Honorato, R. V. et al. The HADDOCK2.4 web server for integrative modeling of biomolecular complexes. *Nat. Protoc.* **19**, 3219–3241 (2024).

Acknowledgements

We thank all staff members of the Cryo-EM Center, Southern University of Science and Technology for providing data collection and computation support. We thank Yue Yin of the Mass Spectrometry System at the

National Facility for Protein Science in Shanghai (NFPS), Shanghai Advanced Research Institute, Chinese Academy of Science, China for data collection and analysis. We thank Dr Lin Lin at the core research facilities of Southern University of Science and Technology for the help on mass spectrometry analysis. This work was supported by National Natural Science Foundation of China (32271251 to K.Y., 32371300 to Y.W.), Guangdong Innovative and Entrepreneurial Research Team Program (2021ZT09Y104, 2021QN02Y429 to K.Y.), Shenzhen Science and Technology Program (No. JCYJ20220530115214033, No. KQTD20210811090115021, and No. 20231120160100001 to K.Y.), Guangdong basic and applied basic research foundation (2025A1515011166 to R.M.), China Postdoctoral Science Foundation (2022M721477 to R.M.), and Scientific research funding for postdoctoral researchers staying at Shenzhen (K241387511 to R.M.). K.Y. and F. Z. are investigators of SUSTech Institute for Biological Electron Microscopy. Y.W. acknowledges the computational resources provided by the Information Technology Center and State Key Lab of Computer-Aided Design (CAD) & Computer Graphics (CG) of Zhejiang University.

Author contributions

R.M. and B.D. purified the proteins and conducted biochemical studies. C.S. and Y.W. performed the normal mode analysis and integrative structural modeling. L.W. and F.Z. contributed to data collection. R.M. performed the cryo-EM analysis and the model building. J.H. and H.G. processed the mass spectrometry data. R.M. and K.Y. conceived the study and wrote the paper.

Competing interests

The authors declare no competing interests.

Additional information

Supplementary information The online version contains supplementary material available at https://doi.org/10.1038/s41467-025-58363-8.

Correspondence and requests for materials should be addressed to Yong Wang or Kaige Yan.

Peer review information *Nature Communications* thanks Pavel Sinitcy and the other, anonymous, reviewer(s) for their contribution to the peer review of this work. A peer review file is available.